Riemannian Lp Averaging on Lie Group of Nonzero Quaternions

Jesus Angulo

Riemannian L^p Averaging on Lie Group of Nonzero Quaternions

Jesús Angulo

Abstract. This paper discusses quaternion L^p geometric weighting averaging working on the multiplicative Lie group of nonzero quaternions $\mathbb{H}^*$, endowed with its natural bi-invariant Riemannian metric. Algorithms for computing the Riemannian L^p center of mass of a set of points, with $1 \leq p \leq \infty$ (i.e., median, mean, L^p barycenter and minimax center), are particularized to the case of $\mathbb{H}^*$.

Two different approaches are considered. The first formulation is based on computing the logarithm of quaternions which maps them to the Euclidean tangent space at identity $\mathbf{1}$, associated to the Lie algebra of $\mathbb{H}^*$. In the tangent space, Euclidean algorithms for L^p center of mass can be naturally applied. The second formulation is a family of methods based on gradient descent algorithms aiming at minimizing the sum of quaternion geodesic distances raised to power p. These algorithms converges to the quaternion Fréchet-Karcher barycenter ($p = 2$), the quaternion Fermat-Weber point ($p = 1$) and the quaternion Riemannian 1-center ($p = +\infty$).

Besides giving explicit forms of these algorithms, their application for quaternion image processing is shown by introducing the notion of quaternion bilateral filtering.

Keywords. Lie group of nonzero quaternions, quaternion averaging, Log-Euclidean quaternion mean, Riemannian center-of-mass, Fréchet-Karcher barycenter.

1. Introduction

Averaging a finite set of samples is the simplest, but fundamental, operation in signal and image filtering. It allows to deal with denoising and regularizing among other important goals. Let us consider for instance a real valued image $f : \Omega \rightarrow \mathbb{R}$, which maps each pixel to an intensity value, i.e., $\mathbf{x} \mapsto f(\mathbf{x})$. The filtered image according to the kernel $k(\mathbf{x})$ is given by its convolution $(f * k)(\mathbf{x}) = \int_E f(\mathbf{y})k(\mathbf{x} - \mathbf{y})d\mathbf{y}$. For smoothing purposes, $k(\mathbf{x})$ is a real

non-negative valued function which is usually required to be normalized, i.e., $\int_E k(\mathbf{y})d\mathbf{y} = 1$, hence the filter is simply a weighted average. Note also that the canonical case of scale-space image filtering corresponds to the Gaussian kernel, i.e., $k(\mathbf{x}) = 1/(2\pi\sigma^2)\exp\left(-\|\mathbf{x}\|^2/(2\sigma^2)\right)$. This continuous formulation can be easily rewritten for the case of a discrete space of pixels (e.g., for a 2D image $\Omega \subset \mathbb{Z}^2$) as follows:

$$(f * k)(\mathbf{x}) = \sum_{\mathbf{y}\in N(\mathbf{x})} f(\mathbf{y})k(\mathbf{x}-\mathbf{y}),$$

where $N(\mathbf{x})$ is the set of neighbors to pixel $\mathbf{x}$ such that $k(\mathbf{x}) \neq 0$. Consequently, in the case of images valued on a Riemannian manifold $\mathcal{M}$, i.e., $f : \Omega \to \mathcal{M}$, a method to compute the weighted averaging in $\mathcal{M}$ is required to compute $(f * k)(\mathbf{x})$.

In particular, in this paper we are interested in the mathematical setting to process images valued on the space of real quaternions $\mathbb{H}$. More precisely, our framework is the Lie group of nonzero quaternions $\mathbb{H}^* = \mathbb{H} \setminus \{0\}$. When computing averages on points of sets possessing a particular geometry structure, it is desirable to respect this structure. For instance in the Lie group $\mathbb{H}^*$, it would be important to have a notion of average which is stable by the group operation (quaternion product and quaternion inversion in our case). Such a property is ensured for Riemannian L^p center of mass in Lie groups endowed with a bi-invariant Riemannian metric. The Riemannian structure of $\mathbb{H}^*$ is considered in Section 2. In order to have a self-content paper, let us start with a summary of basic quaternion algebra.

Brief remind on quaternion algebra. A quaternion $\mathbf{q} \in \mathbb{H}$ may be represented in a hypercomplex form as $\mathbf{q} = w + xi + yj + zk$ where w, x, y and z are real and i, j and k are operators obeying the following multiplication rules: $i^2 = j^2 = k^2 = ijk = -1$ and $jk = i$, $kj = -i$, $ki = j$, $ik = -j$, $ij = k$, $ji = -k$. A quaternion with $w = 0$ is named a pure quaternion. Real quaternions can be embedded in $\mathbb{R} \times \mathbb{R}^3$, and be represented as $\mathbf{q} = (w, \mathbf{v})$, by its scalar part w and its vector part $\mathbf{v} = (x, y, z)$, the latter corresponds to the "vectorization" of the imaginary part. Using this representation, multiplication of two quaternions is defined by $\mathbf{q}_1\mathbf{q}_2 = (w, \mathbf{v})$, where $w = w_1w_2 - \mathbf{v}_1 \cdot \mathbf{v}_2$ and $\mathbf{v} = w_1\mathbf{v}_2 + w_2\mathbf{v}_1 + \mathbf{v}_1 \times \mathbf{v}_2$, $\cdot$ and $\times$ represents the dot product vector and the cross product vector respectively. Quaternion product is not commutative, i.e., $\mathbf{q}_1\mathbf{q}_2 \neq \mathbf{q}_2\mathbf{q}_1$. The norm of a quaternion is defined by $|\mathbf{q}| = \sqrt{w^2 + x^2 + y^2 + z^2}$. A quaternion with a norm equal to 1 is named a unit quaternion. The conjugate of a quaternion is defined by $\mathbf{q}^* = w - xi - yj - zk$. The multiplicative inverse of a quaternion is defined as $\mathbf{q}^{-1} = \mathbf{q}^*/|\mathbf{q}|$, such that $\mathbf{q}\mathbf{q}^{-1} = \mathbf{1}$.

The polar representation of a quaternion is given by $\mathbf{q} = |\mathbf{q}|e^{\mathbf{n}\theta} = |\mathbf{q}|(\cos\theta + \mathbf{n}\sin\theta)$, where $\mathbf{n} = \frac{xi+yj+zk}{\xi}$, $\xi = \sqrt{x^2+y^2+z^2}$ and $\theta = \arccos\left(\frac{w}{|\mathbf{q}|}\right)$. It will be denoted by $U\mathbf{q}$ the unit quaternion associated to $\mathbf{q}$, i.e., $U\mathbf{q} = \frac{\mathbf{q}}{|\mathbf{q}|}$, thus $U\mathbf{q} = e^{\mathbf{n}\theta}$. The power of a quaternion to a

real $\alpha \in \mathbb{R}$ is easily obtained by the polar representation $\mathbf{q}^\alpha = |\mathbf{q}|^\alpha e^{\mathbf{n}\alpha\theta} = |\mathbf{q}|^\alpha(\cos(\alpha\theta) + \mathbf{n}\sin(\alpha\theta))$.

State-of-the-art on quaternion averaging. It is well known that 3D rotations can be formulated by the product of unit quaternions. Rotation averaging, and consequently unit quaternion averaging, have been the subject of many research works [43] [19] [26]. In addition, averaging in the Special Orthogonal Group SO(3) using matrix averaging as well as averaging in $\mathbb{S}^3$ are also related to unit quaternion averaging [39] [35] [32] [24] [41][22] [27]. Averaging unit quaternions has also been considered in [18], as a particular case of averaging in Clifford groups (the group Spin(3)) by considering approximation of the Riemannian means by Euclidean means on Clifford algebra. However, from our viewpoint, the issue of quaternion center of mass is not limited to unit quaternions and it is still a relatively open issue, with potential applications for instance in 4-variate image filtering.

Organization of the paper. Inspired by the recent works on geometric averaging of (Hermitian) Positive Definite Matrices using differential geometry tools [36, 8, 23, 15, 10, 11], we introduce in Section 3 of the paper two approaches of nonzero quaternion L^p geometric weighting averaging working on the Riemannian framework of $\mathbb{H}^*$. The first formulation is based on computing the logarithm of quaternions which maps them to the Euclidean tangent space at identity $\mathbf{1}$, associated to the Lie algebra of $\mathbb{H}^*$. In the tangent space, Euclidean algorithms for L^p center of mass can be naturally applied. In the second formulation, a family of methods based on gradient descent algorithms aiming at minimizing the sum of quaternion geodesic distances raised to power p is considered. These algorithms converges to the quaternion Fréchet-Karcher barycenter ($p = 2$), the quaternion Fermat-Weber point ($p = 1$) and the quaternion Riemannian 1-center ($p = +\infty$).

Besides giving explicit forms of these algorithms, their application for quaternion image processing is shown in Section 4, introducing the notion of quaternion bilateral filtering. The performance of this approach of locally adaptive (spatially-variant) nonlinear filtering is illustrated using RGB color images, but also RGB-NIR images and RGB-Depth ones where the quaternionic image representation allows to deal simultaneously with four components.

2. Multiplicative Lie Group of Nonzero Quaternions

Any Lie group is an algebraic group that also possesses the structure of a (smooth) differential manifold. In the present section, the Riemannian geometry of the Lie group $\mathbb{H}^*$ is recalled. We start with the basic ingredients from quaternion calculus, which are required to precise the Riemannian manifold endowing $\mathbb{H}^*$: the exponential and logarithm of a quaternion.

2.1. Exponential and logarithm of quaternion

Exponential of a quaternion $\mathbf{q} \in \mathbb{H}$ is defined using the power series representation as $\exp(\mathbf{q}) = 1 + \frac{\mathbf{q}}{1!} + \frac{\mathbf{q}^2}{2!} + \cdots + \frac{\mathbf{q}^n}{n!} + \cdots$ which can be expressed in a closed-form using a similitude to Moivre's formula [4]:

$$\exp(\mathbf{q}) = \exp(w, \mathbf{v}) = e^w \left(\cos|\mathbf{v}|, \sin|\mathbf{v}| \frac{\mathbf{v}}{|\mathbf{v}|} \right). \tag{2.1}$$

The logarithm of a quaternion is defined as the inverse function $\log(\mathbf{q}) = \exp^{-1}(\mathbf{q})$, which is given by the expression:

$$\log(\mathbf{q}) = \log(w, \mathbf{v}) = \left(\log|\mathbf{q}|, \frac{\mathbf{v}}{|\mathbf{v}|} \arccos\left(\frac{w}{|\mathbf{q}|} \right) \right). \tag{2.2}$$

By definition of logarithm, it is required that $|\mathbf{q}| \neq 0$. Therefore quaternionic logarithm is defined only for nonzero quaternions, i.e., $\log(\mathbf{q})$ exists $\forall \mathbf{q} \in \mathbb{H}^*$. The exponential mapping is onto but not one-to-one (it is a multi-valued function). That involves that $\log(\exp(\mathbf{q})) = \mathbf{q}$ is already not always true for complex numbers; however, $\exp(\log(\mathbf{q})) = \mathbf{q}$ always holds for all branches of the logarithm, because it is essentially the definition of the log.

Let us consider two special cases of exponential/logarithm of a quaternion. If we have a pure quaternion $\mathbf{q} = (0, \mathbf{v})$, its exponential mapping produces a unit vector in $\mathbb{R}^4$, or more formally $\exp(0, \mathbf{v}) : \mathbb{R}^3 \rightarrow \mathbb{S}^3$. The logarithm of a pure quaternion is given by $\log(0, \mathbf{v}) = \left(\log|\mathbf{v}|, \frac{\pi}{2} \frac{\mathbf{v}}{|\mathbf{v}|} \right)$, i.e., the modulus and unit direction of vector in $\mathbb{R}^3$ are decoupled. For the case of a unit quaternion $\mathbf{q}$, such that $|\mathbf{q}| = 1$, its logarithm gives $\log(w, \mathbf{v}) = \left(0, \frac{\mathbf{v}}{|\mathbf{v}|} \arccos(w) \right)$.

2.2. Riemannian geometry structure of $\mathbb{H}^*$

The set $\mathbb{H}^*$ of nonzero quaternions is a Lie group under quaternion multiplication. The line element of the standard bi-invariant metric is given by

$$ds^2_{\mathbb{H}^*} = \left(\frac{d|\mathbf{q}|}{|\mathbf{q}|} \right)^2 + (dU\mathbf{q})^2. \tag{2.3}$$

It is the metric such that the left invariant 1-form $\omega = \mathbf{q}^{-1} d\mathbf{q}$ with values in $\mathbb{H}^* \rightarrow \mathbb{H}$ is an isometry at every point, i.e., for every $\mathbf{p}$ nonzero quaternion, $\omega_{\mathbf{p}} : \mathbb{H}^* \rightarrow \mathbb{H}$ induces an isometry between $T_{\mathbf{p}}\mathbb{H}$ under this metric with $\mathbb{H}^*$ given the standard quaternion norm. This metric (which is complete and homogeneous) is a product metric:

$$ds^2_{\mathbb{H}^*} = ds^2_{\mathbb{R}_+} + ds^2_{\mathbb{S}^3}.$$

The underlying Riemannian manifold is isometric to the product manifold $\mathbb{R}_+ \times \mathbb{S}^3$ with the canonical metrics. Thus, as a product manifold, it is simply connected and complete but it is not compact. Also observe that $\left(\mathbb{R}_+, ds^2_{\mathbb{R}_+} \right)$ has zero sectional curvature and that $\left(\mathbb{S}^3, ds^2_{\mathbb{S}^3} \right)$ has constant sectional curvature 1. It can be proved that, see for instance [49], given two Riemannian

manifolds $\mathcal{M}, \mathcal{N}$ such that the sectional curvatures verify $0 \leq K_{\mathcal{M}}, K_{\mathcal{N}} \leq C$, where $C \geq 0$ is a constant, then the sectional curvatures of the product manifold $\mathcal{M} \times \mathcal{N}$ also verify $0 \leq K_{\mathcal{M}\times\mathcal{N}} \leq C$. Hence, the sectional curvature of $\mathbb{H}^*$ is nonnegative and bounded by 1: $0 \leq K_{\mathbb{H}^*} \leq 1$.

We notice that the set of unit quaternions which is isomorphic to $\mathbb{S}^3$ is a subgroup of $\mathbb{H}^*$. The isomorphism of unit quaternions to groups Spin(3) and SU(2) are also well known.

Exponential function of pure quaternions and its inverse logarithm provide a correspondence between $\mathbb{S}^3$ and its tangent space $T_{\mathbf{1}}\mathbb{S}^3 \equiv \mathbb{R}^3$ at the identity $\mathbf{1} = (1, 0, 0, 0)$. That involves that for any given unit $\mathbf{q}$ in the neighborhood of the identity, there exists $\mathbf{v} \in T_{\mathbf{1}}\mathbb{S}^3$ which is mapped to $\mathbf{q}$ by $\mathbf{q} = \exp(\mathbf{v})$.

More generally, the exponential map $\mathrm{Exp}_{\mathbf{q}}$ and the logarithmic map $\mathrm{Log}_{\mathbf{q}}$ from the Riemannian manifold associated to $\mathbb{H}^*$ onto the vector tangent space $T_{\mathbf{q}}\mathbb{H}^*$ at a given quaternion $\mathbf{q}$ are respectively:

$$\mathrm{Exp}_{\mathbf{q}} \;:\; \begin{cases} T_{\mathbf{q}}\mathbb{H}^* \cong \mathbb{H} & \longrightarrow \quad \mathbb{H}^* \\ \eta = (\eta_1, \eta_2, \eta_3, \eta_4) & \mapsto \quad \mathrm{Exp}_{\mathbf{q}}(\eta) = \mathbf{q}\exp(\eta) \end{cases}$$

$$\mathrm{Log}_{\mathbf{q}} \;:\; \begin{cases} \mathbb{H}^* & \longrightarrow \quad T_{\mathbf{q}}\mathbb{H}^* \cong \mathbb{H} \\ \mathbf{p} & \mapsto \quad \mathrm{Log}_{\mathbf{q}}(\mathbf{p}) = \log\left(\mathbf{q}^{-1}\mathbf{p}\right) \end{cases}$$

Note that we assume that the tangent space to any element of $\mathbb{H}^*$ is identified to the linear vector space $\mathbb{R}^4$ [1], i.e., $T_{\mathbf{q}}\mathbb{H}^* \cong \mathbb{H} \cong \mathbb{R}^4$. In fact, the Lie algebra $\mathfrak{g}_{\mathbb{H}^*}$ of the group $\mathbb{H}^*$ is isomorphic to $\mathfrak{g}_{\mathbb{H}^*} \cong \mathbb{R} \oplus \mathfrak{so}(3)$ [12].

In this framework, the Riemannian distance between two quaternions $\mathbf{q}_1$ and $\mathbf{q}_2$ in $(\mathbb{H}^*, ds_{\mathbb{H}^*})$ is the length of the shortest geodesic path on the manifold $\mathbb{H}^*$ between both quaternions and is given by

$$\mathrm{dist}_{\mathbb{H}^*}(\mathbf{q}_1, \mathbf{q}_2) = \|\mathrm{Log}_{\mathbf{q}_1}(\mathbf{q}_2)\| = \left\|\log\left(\mathbf{q}_1^{-1}\mathbf{q}_2\right)\right\|. \tag{2.4}$$

This expression is well known in the case of unit quaternions since it is the Riemannian metric of $\mathbb{S}^3$. Using the polar representation, it can be rewritten as

$$\mathrm{dist}_{\mathbb{H}^*}(\mathbf{q}_1, \mathbf{q}_2)^2 = |\log(|\mathbf{q}_2|) - \log(|\mathbf{q}_1|)|^2 + \|\log\left(U\mathbf{q}_1^* U\mathbf{q}_2\right)\|^2.$$

The geodesic distance of $\mathbb{H}^*$ is bi-invariant, that is, for any $\mathbf{p}, \mathbf{r} \in \mathbb{H}^*$

$$\begin{aligned} \mathrm{dist}_{\mathbb{H}^*}(\mathbf{p}\mathbf{q}_1, \mathbf{p}\mathbf{q}_2) &= \mathrm{dist}_{\mathbb{H}^*}(\mathbf{q}_1\mathbf{r}, \mathbf{q}_2\mathbf{r}) = \mathrm{dist}_{\mathbb{H}^*}(\mathbf{p}\mathbf{q}_1\mathbf{p}^{-1}, \mathbf{p}\mathbf{q}_2\mathbf{p}^{-1}) \\ &= \mathrm{dist}_{\mathbb{H}^*}(\mathbf{q}_1, \mathbf{q}_2). \end{aligned}$$

Other interesting property is associated to the invariance to inversion:

$$\mathrm{dist}_{\mathbb{H}^*}(\mathbf{q}_1^{-1}, \mathbf{q}_2^{-1}) = \mathrm{dist}_{\mathbb{H}^*}(\mathbf{q}_1, \mathbf{q}_2).$$

The fact that in general $\mathbf{q}_1^{-1}\mathbf{q}_2 \neq \mathbf{q}_2\mathbf{q}_1^{-1}$ does not affect the distance (2.5) since by the bi-invariance we have $\left\|\log\left(\mathbf{q}_1^{-1}\mathbf{q}_2\right)\right\| = \left\|\log\left(\mathbf{q}_1\mathbf{q}_2^{-1}\right)\right\|$. We propose to use a symmetrized version of the geodesic distance between two quaternions in $\mathbb{H}^*$ as follows:

$$\mathrm{dist}_{\mathbb{H}^*}(\mathbf{q}_1, \mathbf{q}_2) = \left\|\log\left(\mathbf{q}_1^{-\frac{1}{2}}\mathbf{q}_2\mathbf{q}_1^{-\frac{1}{2}}\right)\right\| \tag{2.5}$$

From the differential geometry of $\mathbb{H}^*$, we can also define the geodesic parameterized by the length, $t \mapsto \gamma(t)$, joining two quaternions $\mathbf{q}_1$ and $\mathbf{q}_2$ as

$$\gamma(t) = \mathbf{q}_1 \left(\mathbf{q}_1^{-1}\mathbf{q}_2\right)^t \tag{2.6}$$

where $\gamma(0) = \mathbf{q}_1$ and $\gamma(1) = \mathbf{q}_2$. By the properties of quaternion product, equivalent formulations are given by $\gamma(t) = \left(\mathbf{q}_2\mathbf{q}_1^{-1}\right)^t \mathbf{q}_1 = \mathbf{q}_2 \left(\mathbf{q}_2^{-1}\mathbf{q}_1\right)^{1-t}$. Using again the quaternion polar representation, the geodesic is rewritten as

$$\gamma(t) = |\mathbf{q}_1|^{1-t}|\mathbf{q}_2|^t U\mathbf{q}_1 \left(U\mathbf{q}_1^* U\mathbf{q}_2\right)^t$$

Thus, a geodesic path is defined by the product of a geodesic in $\mathbb{R}_+$ (weighted geometric mean of the norms) and a geodesic in $\mathbb{S}^3$. For the case of unit quaternions, this geodesic is just the expression of the spherical linear interpolation (Slerp) [43]. We observe from the polar representation that the geodesic is unique except in case of two quaternions having antipodal unitary parts $U\mathbf{q}_1$ and $U\mathbf{q}_2$ on $\mathbb{S}^3$, which involves the existence of an infinite number of geodesics (great circles) connecting them in $\mathbb{S}^3$.

We propose to reformulate also the geodesic in a symmetrized way as

$$\gamma(t) = \mathbf{q}_1^{\frac{1}{2}} \left(\mathbf{q}_1^{-\frac{1}{2}}\mathbf{q}_2\mathbf{q}_1^{-\frac{1}{2}}\right)^t \mathbf{q}_1^{\frac{1}{2}}; \quad 0 \leq t \leq 1, \tag{2.7}$$

with $\gamma(0) = \mathbf{q}_1$, $\gamma(1) = \mathbf{q}_2$. This kind of symmetrization is similar to the one considered in the Riemannian geometry of positive definite matrices [13], and it is inspired from operators algebras in mathematical physics. From a numerical viewpoint, we have observed that this symmetrization produces more numerically stable results in the gradient descent algorithms. Using logarithm and exponential of quaternions, the symmetrized geodesic (2.7) is by definition of the power equivalent to

$$\gamma(t) = \mathbf{q}_1^{\frac{1}{2}} \exp\left(t \log\left(\mathbf{q}_1^{-\frac{1}{2}}\mathbf{q}_2\mathbf{q}_1^{-\frac{1}{2}}\right)\right) \mathbf{q}_1^{\frac{1}{2}}, \tag{2.8}$$

which in this form will appear below in the algorithms for averaging.

3. Riemannian L^p Averaging on the Quaternion Lie Group $\mathbb{H}^*$

Averaging on a Lie group may be regarded as weighted averaging on its associated algebra [23]. In fact, working on the Riemannian manifold associated to the Lie group, averaging algorithms are naturally defined using differential geometry tools. This section starts with a summary of the definition of L^p center of mass for a set of sample points in a Riemannian manifold. Then, as a first tentative to instantiate these statistics to the case of nonzero quaternions, the Log-Euclidean averaging framework is considered for $\mathbb{H}^*$. Finally, algorithms from a genuine framework of Riemannian L^p averaging in $\mathbb{H}^*$ are introduced.

3.1. Riemannian L^p center of mass

Let $\mathcal{M}$ be a Riemannian manifold and let $d(x, y)$ be the Riemannian distance function on $\mathcal{M}$. Given N points $x_1, x_2, \cdots, x_N \in \mathcal{M}$ and the corresponding positive real weights $\alpha_1, \alpha_2, \cdots, \alpha_N$, with $\sum_{1 \leq i \leq N} \alpha_i = 1$, the Riemannian L^p center of mass, with $p \in [1, +\infty)$, is defined as the minimizer of the sum of p powered distances function

$$c_p = \arg\min_{x \in \mathcal{M}} \sum_{i=1}^{N} \alpha_i d^p(x, x_i). \tag{3.1}$$

This general definition, includes two cases of well known Riemannian statistics. The geometric mean (Karcher-Fréchet barycenter) is the minimizer of the sum-of-squared distances function

$$\mu = \arg\min_{x \in \mathcal{M}} \sum_{i=1}^{N} \alpha_i d^2(x, x_i), \tag{3.2}$$

and the geometric median (Fermat-Weber point) is the minimizer of sum-of-distances function

$$m = \arg\min_{x \in \mathcal{M}} \sum_{i=1}^{N} \alpha_i d(x, x_i). \tag{3.3}$$

Additionally, the particular case $p = +\infty$, known as Riemannian 1-center (minimax center), corresponds to the minimizer of max-of-distances function

$$c_\infty = \arg\min_{x \in \mathrm{supp}_{\mathcal{M}}(\{x_i\})} \left[\max_{1 \leq i \leq N} d(x, x_i) \right], \tag{3.4}$$

where $\mathrm{supp}_{\mathcal{M}}(\{x_i\})$ is the closure of the convex hull on $\mathcal{M}$ of $\{x_i\}_{i=1}^N$.

To have an appropriate definition of Riemannian center of mass, it should be assumed that points $x_i \in \mathcal{M}$ lie in a convex set $U \in \mathcal{M}$, i.e., any two points in U are connected by a unique shortest geodesic lying entirely in U. The diameter of U, denoted $\mathrm{diam}(U)$, is the maximal distance between any two points in U. We notice that the squared geodesic distance function and the geodesic distance function in U are convex. Existence and uniqueness of geometric mean (3.2) and geometric median (3.3) have been widely considered: both exist and are unique if the sectional curvatures of $\mathcal{M}$ are nonpositive, or if the sectional curvatures of $\mathcal{M}$ are bounded above by $\Delta > 0$ and $\mathrm{diam}(U) < \pi/(2\sqrt{\Delta})$ [29, 30, 24]. More recently, the existence and uniqueness for the Riemannian L^p center of mass, $1 \leq p \leq \infty$ have been studied in [2]. We can find also more recent results on existence and uniqueness, including also practical algorithms for L^2 [14, 34], for L^1 [48], for L^p [2, 3] and for L^∞ [6]. We can mention also some results on stochastic algorithms (avoiding to compute the gradient to minimize) [5, 16].

3.2. Log-Euclidean L^p averaging on $\mathbb{H}^*$

The idea of this averaging approach is inspired from the framework of Log-Euclidean mean for symmetric positive-definite matrices, introduced and studied in [7, 8]. The rationale behind the framework is to compute the

arithmetic average in Lie algebra $\mathfrak{g}_{\mathbb{H}^*}$, i.e., to work on the tangent space at the identity.

Log-Euclidean mean. Lets consider a set N of nonzero quaternions, denoted by $\mathfrak{Q} = \{\mathbf{q}_i\}_{i=1}^N$, with positive weights $\mathbf{A} = \{\alpha_i\}_{i=1}^N$, $\alpha_i \geq 0$. The Log-Euclidean mean on $\mathbb{H}^*$ is defined as the weighted averaged in the Euclidean tangent space

$$\bar{\mathbf{q}} = \mathbb{E}_{LE}(\mathfrak{Q}, \mathbf{A}) = \exp\left(\sum_{i=1}^{N} \alpha_i \log(\mathbf{q}_i)\right) \tag{3.5}$$

It can be easily rewritten as

$$\bar{\mathbf{q}} = \prod_{i=1}^{N} |\mathbf{q}_i|^{\alpha_i} \left(\cos|\bar{\mathbf{v}}| + \sin|\bar{\mathbf{v}}| \frac{\bar{\mathbf{v}}}{|\bar{\mathbf{v}}|}\right),$$

where

$$\bar{\mathbf{v}} = \sum_{i=1}^{N} \frac{\alpha_i}{|\mathbf{v}_i|} \arccos\left(\frac{w_i}{\sqrt{w_i^2 + |\mathbf{v}_i|^2}}\right) \mathbf{v}_i.$$

Thus, $\bar{\mathbf{q}}$ can be interpreted as the quaternion given, on the one hand, by the weighted geometric mean of the norms of quaternions, and on the other hand, the normalized vector part (or imaginary part) of the quaternion as the expectation computed in the tangent space at the north pole of $\mathbb{S}^3$. In fact, we can see that the Log-Euclidean mean is the Riemannian equivalent of the arithmetic mean in the sense that

$$\mathbb{E}_{LE}(\mathfrak{Q}, \mathbf{A}) = \arg\min_{\mathbf{q} \in \mathbb{H}^*} \sum_{i=1}^{N} \alpha_i \mathrm{dist}_{LE}^2(\mathbf{q}, \mathbf{q}_i) = \bar{\mathbf{q}},$$

where $\mathrm{dist}_{LE}(\mathbf{q}_1, \mathbf{q}_2) = \|\log(\mathbf{q}_1) - \log(\mathbf{q}_2)\|$ is the Log-Euclidean metric associated to the Log-Euclidean geodesic $\gamma_{LE}(t) = \exp((1-t)\log(\mathbf{q}_1) + t\log(\mathbf{q}_2))$, which obviously does not correspond to the quaternion geodesic metric $\gamma(t)$ given by expression (2.6).

Log-Euclidean median. A similar idea can be used to compute the Log-Euclidean median by working on the vector space associated to $\mathfrak{g}_{\mathbb{H}^*}$. However, the median in vector spaces does not have a closed formula. Given a discrete set of N samples $x_1, x_2, \cdots, x_N$, with each $x_i \in \mathbb{R}^n$, the geometric median (Fermat-Weber point or 1-median) is defined as

$$m = \arg\min_{x \in \mathbb{R}^n} \sum_{i=1}^{M} \|x_i - x\|_2.$$

In Euclidean spaces, it has been shown that no explicit formula, nor any exact algorithm, exists in general. The most popular technique to obtain the vector median is Weiszfeld algorithm [47], later improved in various works [33, 37]. It consists in iteratively weighted least squares updating the estimate m^k of the median, where the weights are inversely proportional to the distances

from the current estimate to the samples

$$m^{k+1} = \left(\sum_{i=1 \ x_i \neq m^k}^{N} \frac{x_i}{\|x_i - m^k\|} \right) \left(\sum_{i=1 \ x_i \neq m^k}^{N} \frac{1}{\|x_i - m^k\|} \right)^{-1}.$$

Therefore, the Log-Euclidean quaternion median (L^1 average) of a set of N nonzero quaternions $\mathfrak{Q} = \{\mathbf{q}_i\}_{i=1}^N$ with positive weights $\mathbf{A} = \{\alpha_i\}_{i=1}^N$, $\alpha_i \geq 0$, is defined as the weighted median in the Euclidean tangent space at identity $\mathbf{1}$, i.e.,

$$\tilde{\mathbf{q}} = \mathbb{M}_{LE}(\mathfrak{Q}, \mathbf{A}) = \exp(\tilde{\eta}), \tag{3.6}$$

where $\tilde{\eta}$ is the median estimate obtained by Weiszfeld algorithm, i.e., $\tilde{\eta} = \eta^k$ such that $\|\eta^{k+1} - \eta^k\| < \epsilon$ and

$$\eta^{k+1} = \left(\sum_{i=1 \ \eta_i \neq \eta^k}^{N} \alpha_i \frac{\eta_i}{\|\eta_i - \eta^k\|} \right) \left(\sum_{i=1 \ \eta_i \neq \eta^k}^{N} \frac{\alpha_i}{\|\eta_i - \eta^k\|} \right)^{-1}, \tag{3.7}$$

where

$$\eta_i = \log(\mathbf{q}_i) = \left(\log|\mathbf{q}_i|, \frac{\mathbf{v}_i}{|\mathbf{v}_i|} \arccos\left(\frac{w_i}{|\mathbf{q}_i|} \right) \right), \ \eta_i \in T_{\mathbf{1}}\mathbb{H}^* \cong \mathbb{R}^4. \tag{3.8}$$

Log-Euclidean minimax center. Furthermore, the Log-Euclidean framework naturally generalizes to the 1-center (center of mass with $p = \infty$). Given a discrete set of N samples $x_1, x_2, \cdots, x_N$, with each $x_i \in \mathbb{R}^n$, the 1-center (Sylvester point or minimax center) is defined as

$$c_\infty = \arg\min_{x \in \mathbb{R}^n} \max_{1 \leq i \leq N} \|x_i - x\|_2,$$

and corresponds to finding the unique smallest enclosing ball in $\mathbb{R}^n$ that contains all the given points. Computing the smallest enclosing ball in Euclidean spaces is intractable in high dimension, but efficient approximation algorithms have been proposed. The Bădoiu and Clarkson algorithm [9] leads to a fast and simple approximation (of known precision ϵ after a given number of iterations $\lceil \frac{1}{\epsilon^2} \rceil$ using the notion of core-set, but independent of dimensionality n): Initialize the minimax center c_∞^1 with an arbitrary point of $\{x_i\}_{1 \leq i \leq N}$, then iteratively update the center

$$c_\infty^{k+1} = c_\infty^k + \frac{f^k - c_\infty^k}{k+1},$$

where f^k is the farthest point of set $\{x_i\}_{1 \leq i \leq N}$ to c_∞^k. The Log-Euclidean quaternion 1-center (or L^∞ average) of $\mathfrak{Q} = \{\mathbf{q}_i\}_{i=1}^N$ is defined as the 1-center in the Euclidean tangent space at $\mathbf{1}$

$$\breve{\mathbf{q}} = \mathbb{D}_{LE}(\mathfrak{Q}) = \exp(\breve{\eta}),$$

where $\breve{\eta}$ is the estimate of the center of the unique smallest enclosing ball in $\mathbb{R}^4$, i.e., $\breve{\eta} = \eta^k$ according to the algorithm

1. $\eta^1 = \eta_1$;

2. Iteratively update

$$\eta^{k+1} = \eta^k + \frac{\phi^k - \eta^k}{k+1};$$

where $\phi^k = \arg\max_{\eta_i,\, 1\leq i\leq N} \|\eta_i - \eta^k\|$, until $\|\eta^{k+1} - \eta^k\| < \epsilon$.

Note that the vectors η_i are obtained from (3.8).

Properties of Log-Euclidean L^p averages. Log-Euclidean L^p averages are invariant to quaternion inversion: the inversion of quaternion is the multiplication by -1 of their logarithms, i.e., $\mathbf{q} \mapsto \mathbf{q}^{-1} \Rightarrow \log(\mathbf{q}) \mapsto -\log(\mathbf{q})$. More generally, the Log-Euclidean L^p averages are invariant to scaling (multiplication by a real factor involves a translation in the domain of logarithms, i.e., $\mathbf{q} \mapsto \alpha\mathbf{q} \Rightarrow \log(\mathbf{q}) \mapsto \log(\alpha) + \log(\mathbf{q})$. However, Log-Euclidean L^p averages are not invariant to rotation transformation. Indeed, quaternion rotation is given by the product of unit quaternions, i.e., $\mathbf{q} \mapsto \mathbf{u}\mathbf{q}\mathbf{u}^{-1}$, but $\log(\mathbf{u}\mathbf{q}\mathbf{u}^{-1})$ is not necessarily equal to $\log(\mathbf{u}) + \log(\mathbf{q}) - \log(\mathbf{u})$. It is well known in the case of positive matrices that the Log-Euclidean L^p averages are not order-preserving (since the exponential map is not order-preserving) [13]. A similar behavior is observed for the case of nonzero quaternions.

3.3. Riemannian L^p averaging in $\mathbb{H}^*$

We propose now to compute efficiently a precise estimation to the Riemannian mean quaternion underlying the minimization of the quaternion geodesic distance, i.e.,

$$\mathbb{E}(\mathfrak{Q}, \mathbf{A}) = \arg\min_{\mathbf{q}\in\mathbb{H}} \sum_{i=1}^{N} \alpha_i \operatorname{dist}^2_{\mathbb{H}^*}(\mathbf{q}, \mathbf{q}_i),$$

with $\operatorname{dist}_{\mathbb{H}^*}(\mathbf{q}_1, \mathbf{q}_2) = \left\| \log\left(\mathbf{q}_1^{-\frac{1}{2}} \mathbf{q}_2 \mathbf{q}_1^{-\frac{1}{2}} \right) \right\|$. The case when $N = 2$ is explicitly given by the geodesic path (2.8) at $t = 1/2$. Unfortunately, this closed form of the geometric mean of two quaternions on $\mathbb{H}^*$ cannot be generalized to more than two quaternions. We propose to use a gradient descent algorithm to estimate $\mathbb{E}(\mathfrak{Q}, \mathbf{A})$.

Riemannian mean. Given a manifold $\mathcal{M}$, Fréchet-Karcher flow [25] [29] is an intrinsic gradient flow on $\mathcal{M}$ that converges to the L^2 center of mass, called Fréchet-Karcher barycenter. In the discrete case, the L^2 center of mass for a finite set of N points on $\mathcal{M}$ is given by:

$$\mu_{k+1} = \operatorname{Exp}_{\mu_k}\left(\beta \sum_{i=1}^{N} \operatorname{Log}_{\mu_k}(x_i) \right),$$

where $\operatorname{Exp}_\mu(\cdot)$ is the exponential map and $\operatorname{Log}_\mu(a) \in T_\mu\mathcal{M}$ is the tangent vector at $\mu \in \mathcal{M}$ of the geodesic from μ to a; and where $\beta > 0$ is the step parameter of the gradient descent.

Coming back to the case of Lie group $\mathbb{H}^*$, the geometric barycenter $\mathbb{E}(\mathfrak{Q}, \mathbf{A})$ can be computed by the following gradient Fréchet-Karcher flow

$$\bar{\mathbf{q}}_{k+1} = \bar{\mathbf{q}}_k^{\frac{1}{2}} \exp\left(\beta \sum_{i=1}^{N} \alpha_i \log\left(\bar{\mathbf{q}}_k^{-\frac{1}{2}} \mathbf{q}_i \bar{\mathbf{q}}_k^{-\frac{1}{2}}\right)\right) \bar{\mathbf{q}}_k^{\frac{1}{2}}. \tag{3.9}$$

which is iterated until convergence (i.e., $\mathrm{dist}(\bar{\mathbf{q}}_{k+1}, \bar{\mathbf{q}}) \leq \epsilon$) and where we fix $\beta = \frac{1}{N}$. This algorithm of geometric barycenter for quaternions is structurally similar to those introduced recently for covariance matrices in the framework of information geometry [10, 11]. If we remind that the Riemannian manifold associated to $\mathbb{H}^*$ has a nonnegative bounded by 1 sectional curvature, the uniqueness of quaternion Fréchet-Karcher barycenter depends on the diameter of the geodesic ball set containing the quaternions to be averaged. This can be a problem if the points are very spread on $\mathbb{H}^*$. A critical concern for the uniqueness of Fréchet-Karcher barycenter is the case of antipodal quaternions. However, for the applicative framework considered in this work, where the 4-variate image pixels are always nonnegative valued, the set of quaternions $\{\mathbf{q}_i\}$ lies in the positive orthant of $\mathbb{H}^*$.

In any case, to guarantee a fast convergence of the algorithm (3.9) to a (local) minimum, it is needed that the initialization is close to the final average. Hence, we propose the initialization to the Log-Euclidean mean; i.e., $\bar{\mathbf{q}}_{k=1} = \exp\left(\frac{1}{N} \sum_{i=1}^{N} \alpha_i \log(\mathbf{q}_i)\right)$.

With respect to the state-of-the-art, we remark also that expression (3.9) of Fréchet-Karcher barycenter is equivalent to the gradient descent algorithm A1 in [19] for averaging unit quaternions in $\mathbb{S}^3$. Note that the algorithm in [19] was proposed for spherical weighted averages in $\mathbb{S}^d$ using the exponential map and its inverse map in spherical coordinates.

Riemannian median. Fermat-Weber point, as the geometric median (3.3), can be also extended to quaternions. Indeed, for any Riemannian manifold $\mathcal{M}$, the gradient of the Riemannian sum-of-distances function is given by

$$\nabla f(x)|_{x \in U;\, x \neq x_i} = -\sum_{i=1}^{N} w_i \frac{\mathrm{Log}_x(x_i)}{d(x, x_i)} = -\sum_{i=1}^{N} w_i \frac{\mathrm{Log}_x(x_i)}{\| \mathrm{Log}_x(x_i) \|}$$

With this result, Weiszfeld-Ostresh algorithm for Riemannian manifolds is written as [24]:

$$m^{k+1} = \mathrm{Exp}_{\mathrm{m}^k}\left(\left(\beta \sum_{i \in I_k} w_i \frac{\mathrm{Log}_{m^k}(x_i)}{\| \mathrm{Log}_{m^k}(x_i) \|}\right)\left(\sum_{i \in I_k} \frac{w_i}{\| \mathrm{Log}_{m^k}(x_i) \|}\right)^{-1}\right)$$

where $I_k = \left\{i \in [1, N] :\ m^k \neq x_i\right\}$ and $0 \leq \beta \leq 2$. Now, by straightforward substitution, we obtain that the geometric median of a finite set of N quaternions, $\mathbb{M}(\mathfrak{Q}, \mathbf{A})$, can be computed as follows

$$\bar{\mathbf{q}}_{k+1} = \bar{\mathbf{q}}_k^{\frac{1}{2}} \exp\left(\left(\beta_k \sum_{i \in N_k} \alpha_i \frac{\log\left(\bar{\mathbf{q}}_k^{-\frac{1}{2}} \mathbf{q}_i \bar{\mathbf{q}}_k^{-\frac{1}{2}}\right)}{\| \log\left(\bar{\mathbf{q}}_k^{-\frac{1}{2}} \mathbf{q}_i \bar{\mathbf{q}}_k^{-\frac{1}{2}}\right) \|}\right)\left(\sum_{i \in N_k} \frac{\alpha_i}{\| \log\left(\bar{\mathbf{q}}_k^{-\frac{1}{2}} \mathbf{q}_i \bar{\mathbf{q}}_k^{-\frac{1}{2}}\right) \|}\right)^{-1}\right) \bar{\mathbf{q}}_k^{\frac{1}{2}} \tag{3.10}$$

where $N_k = \{i \in [1, N] : \mathbf{q}_k \neq \mathbf{q}_i\}$. It was proven in [24] that the Riemannian Weiszfeld-Ostresh algorithm converges to the geometric median $\lim_{k\to\infty} m^k = m$, for $0 \leq \beta \leq 2$ if sectional curvatures of $\mathcal{M}$ are nonnegative and bounded. These requirements fits with the geometry of $\mathbb{H}^*$ and consequently the use for nonzero quaternions is particularly well adapted. More precisely, we propose to use as preconized in [48], a step size which is parameterized with respect to the iteration index $\beta_k = \frac{\epsilon}{1+k}$, with $\epsilon = 1$.

Riemannian L^p center of mass. More generally, as studied in [2] for $2 \leq p < \infty$, the Riemannian L^p center of mass c_p (3.1) of a discrete set $\{x_i\}_{i=1}^N \subset \mathcal{M}$ on a manifold $\mathcal{M}$, with respect to weights $0 \leq w_i \leq 1$, $\sum_{i=1}^N w_i = 1$ is the unique zero of the gradient vector field ∇f_p, where

$$\nabla f_p(x) = -\sum_{i=1}^{N} w_i d^{p-2}(x, x_i) \operatorname{Log}_{\mathrm{x}}(x_i)$$

for any $x \in \mathcal{M}$ as long as it is not in the cut locus of any of the data points. The corresponding gradient descent algorithm to find the Riemannian L^p center of mass c_p is given by [3]:

$$c_p^{k+1} = \operatorname{Exp}_{\mathrm{c_p^k}}\left(-\beta_k \nabla f_p(c_p^k)\right) = \operatorname{Exp}_{\mathrm{c_p^k}}\left(\beta_k \sum_{i=1}^{N} w_i d^{p-2}(x, x_i) \operatorname{Log}_{\mathrm{c_p^k}}(x_i)\right).$$

Therefore, the geometric L^p center of mass on $\mathbb{H}^*$ for a finite set of N quaternions, $\mathbb{E}_p(\mathfrak{Q}, \mathbf{A})$, can be computed using the following gradient descent algorithm

$$\bar{\mathbf{q}}_{k+1} = \bar{\mathbf{q}}_k^{\frac{1}{2}} \exp\left(\beta_k \sum_{n=1}^{N} \alpha_i \left\|\log\left(\bar{\mathbf{q}}_k^{-\frac{1}{2}} \mathbf{q}_i \bar{\mathbf{q}}_k^{-\frac{1}{2}}\right)\right\|^{p-2} \log\left(\bar{\mathbf{q}}_k^{-\frac{1}{2}} \mathbf{q}_i \bar{\mathbf{q}}_k^{-\frac{1}{2}}\right)\right) \bar{\mathbf{q}}_k^{\frac{1}{2}}, \tag{3.11}$$

where the step size is parameterized by the iteration index

$$\beta_k = \frac{\epsilon}{1+k}, \quad \text{with } \epsilon = 0.1,$$

thus $\lim_{k\to\infty} \beta_k = 0$.

Riemannian minimax center. For the case of L^∞ Riemannian center of mass (minimum enclosing geodesic ball) as defined in (3.4), there is no canonical algorithm which generalizes the gradient descent algorithms considered for $p \in [1, \infty)$. An extended version of the Euclidean Bădoiu and Clarkson algorithm for 1-center, or minimax center, for Riemannian manifolds has been introduced in a recent work [6]. Let us consider the discrete set $\{x_i\}_{i=1}^N \subset \mathcal{M}$ on a manifold $\mathcal{M}$. First, initialize the center $\bar{x}_\infty$ with a point of set, i.e., $\bar{x}_\infty^1 = x_1$. Then, iteratively update the current minimax center as

$$c_\infty^{k+1} = \text{Geodesic}\left(c_\infty^k, f_i, \frac{1}{1+k}\right),$$

where f_i denotes the farthest point of the set to c_∞^k, and $\text{Geodesic}(p, q, t)$ denotes the intermediate point m on the geodesic passing through p and q such that $\text{dist}(p, m) = t\text{dist}(p, q)$. For the case of a finite set of N nonzero

quaternions $\{\mathbf{q}_i\}_{n=1}^N$, the Riemannian 1-center on $\mathbb{H}^*$ can be computed using the instantiation of Arnaudon-Nielsen algorithm as follows:

1. Initialization: $\bar{\mathbf{q}}_1 = \mathbf{q}_1$
2. Iteratively update
   (a) Obtain the farthest quaternion to the current estimate:
   $$\phi_k = \arg \max_{\mathbf{q}_i,\, 1\leq i\leq N} \| \log \left(\bar{\mathbf{q}}_k^{-\frac{1}{2}} \mathbf{q}_i \bar{\mathbf{q}}_k^{-\frac{1}{2}} \right) \|.$$
   (b) Compute geodesic distance from current center estimation to farthest point:
   $$\mathrm{dist}(\bar{\mathbf{q}}_k, \phi_k) = \| \log \left(\bar{\mathbf{q}}_k^{-\frac{1}{2}} \phi_k \bar{\mathbf{q}}_k^{-\frac{1}{2}} \right) \|.$$
   (c) By bisection search algorithm, find the cut of the geodesic
   $$\gamma(t) = \bar{\mathbf{q}}_k^{\frac{1}{2}} \left(\bar{\mathbf{q}}_k^{-\frac{1}{2}} \phi_k \bar{\mathbf{q}}_k^{-\frac{1}{2}} \right)^t \mathbf{q}_1^{\frac{1}{2}}.$$
   at a value $t = \frac{1}{1+k}$, which gives the quaternion $\bar{\mathbf{q}}_{k+1}$, so that
   $$\mathrm{dist}(\bar{\mathbf{q}}_k, \bar{\mathbf{q}}_{k+1}) = \frac{1}{1+k} \mathrm{dist}(\bar{\mathbf{q}}_k, \phi^k),$$
   where $\mathrm{dist}(\bar{\mathbf{q}}_k, \bar{\mathbf{q}}_{k+1}) = \| \log \left(\bar{\mathbf{q}}_k^{-\frac{1}{2}} \bar{\mathbf{q}}_{k+1} \bar{\mathbf{q}}_k^{-\frac{1}{2}} \right) \|$.

4. Bilateral Filtering of Quaternion Images

The applicative aim of this paper is to illustrate the interest of Riemannian averaging for quaternion image denoising and regularization. In particular, we propose to generalize the notion of bilateral filtering, a very powerful and computationally simple approach for spatially-variant nonlinear filtering framework. We start by formalizing the framework for such images.

Quaternionic images. A 2D quaternion valued image is represented by

$$f_{\mathbf{q}} : \Omega \to \mathbb{H}^*,$$

which corresponds to the function $f_{\mathbf{q}}(\mathbf{x}) = f_w(\mathbf{x}) + f_x(\mathbf{x})i + f_y(\mathbf{x})j + f_z(\mathbf{x})k$, $\mathbf{x} = (x_1, x_2) \in \Omega \subset \mathbb{Z}^2$, i.e., we have a nonzero quaternion at each pixel $\mathbf{x}$ of the image. For instance, a color image of red, green and blue components (RGB), (f_R, f_G, f_B), can be represented by a quaternionic image, i.e., $f_{\mathbf{q}}(\mathbf{x}) = \mathbf{1}(\mathbf{x}) + f_R(\mathbf{x})i + f_G(\mathbf{x})j + f_B(\mathbf{x})k$ (the scalar component is constant and equal to 1). Needless to say that the powerfulness of our image quaternion filtering approach is its ability to deal with images of four components, typically a RGB color image for the imaginary part together with an additional image for the scalar part.

Let us consider two kinds of these images which are nowadays used in the state-of-the-art. On the one hand, using visible and near-infrared (NIR) filters, it is possible to capture color plus thermic images [17]. Fig 1-Top shows an example of such an image, which can be represented as a quaternion image: $f_{\mathbf{q}}(\mathbf{x}) = f_{NIR}(\mathbf{x}) + f_R(\mathbf{x})i + f_G(\mathbf{x})j + f_B(\mathbf{x})k$. On the other hand, the current

technologies of range cameras, such as the popular Kinect one, produce RGB images together with a depth map. An example of RGB+Depth image from database [45] is given in Fig 1-Bottom. The quaternion image is now $f_{\mathbf{q}}(\mathbf{x}) = f_{Depth}(\mathbf{x}) + f_R(\mathbf{x})i + f_G(\mathbf{x})j + f_B(\mathbf{x})k$. But, of course, the key question is the following: what is the justification of working on the multiplicative Lie group of quaternion for processing color, color+temperature and color+distance images.

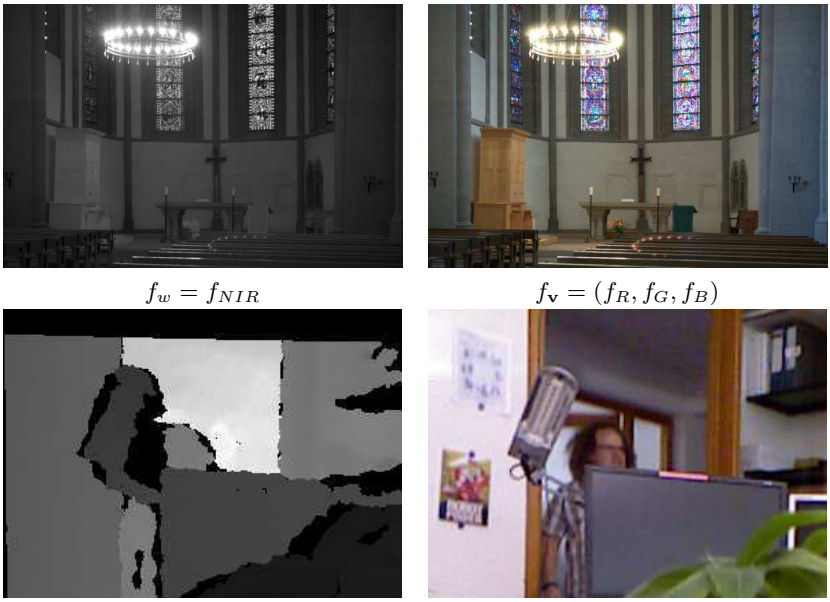

FIGURE 1. Examples of four components image represented by a quaternionic function $f_{\mathbf{q}}(\mathbf{x}) = f_w(\mathbf{x}) + f_x(\mathbf{x})i + f_y(\mathbf{x})j + f_z(\mathbf{x})k$. Top, color + temperature image (RGB+NIR); bottom, color + distance image (RGB+Depth).

Rationale. The classical Weber–Fechner law states that human sensation is proportional to the logarithm of the stimulus intensity. In the case of vision, the eye senses brightness approximately according to Weber–Fechner law over a moderate range. This rationale has been the motivation to introduce a geometry of color spaces that fits the logarithmic perceptual principle. First attempts to deal with were considered by Helmholtz [28] and Schrödinger [42] who introduced color geometries with arc-length for the red, green and blue stimuli of type:

$$ds^2 = \frac{1}{L}\left(c_r\left(\frac{dR}{R}\right)^2 + c_g\left(\frac{dG}{G}\right)^2 + c_b\left(\frac{dB}{B}\right)^2\right), \qquad (4.1)$$

where $L = c_r R + c_g G + c_b B$ and c_r, c_g and c_b are constants. This kind of logarithmic color metrics have been used in modern and theoretically sound image processing based on the Beltrami geometrical framework [44, 31].

By embedding the color images into $\mathbb{H}^*$ according to the metric $ds_{\mathbb{H}^*}$, we have a logarithmic manipulation of the color intensity (or luminance), which corresponds to the norm of the color pixel. In addition, the decoupled chromatic information, given by the unit vector component, is measured by its appropriate metric. This principle of perception-driven processing is also compatible with color + temperature or color + distance images since both temperature and distance are also "logarithmically perceived" as human sensations.

Blurring effect in Riemannian L^p filtering. Hence, geometric L^p center of mass can be used for image filtering by simply computing an average with the quaternion pixels values belonging to a neigbourhood centered at the current pixel.

A comparative series for a RGB+Depth image are given in Figure 2 for the Log-Euclidean framework and in Figure 3 for the Riemannian one. We observe, on the one hand, that the value of p is critical for the effect of filtering. It is well known that, for image filtering, the median estimator ($p = 1$) leads to less blurred contour results than the mean ($p = 2$). This is due to the robustness of median (asymptotic breakdown point equal to 1/2 compared to 1 for the mean [24]), which involves that, in the image zones close to region transitions, the median produces a point belonging to the most represented zone in the filtering window. But, even using the median, the blurring effect is unpleasant. We notice that the minimax center ($p = \infty$) involves a filtering which enhances the outlier pixels values. Obviously, this effect is unappropriate for denoising or standard regularization, however, it is particularly useful for applications such as anomaly detection. On the other hand, concerning the differences between the Log-Euclidean L^p averages against the Riemannian ones, we observe that, for a given filter size, Log-Euclidean produces smoother results associated to the fact that the obtained center of mass does not take into account the precise distribution of the points on the manifold. Nevertheless, in terms of image filtering, results from the Log-Euclidean center of mass are totally acceptable.

Locally adaptive Riemannian L^p averaging. Bilateral filtering [46] is a locally adaptive Gaussian convolution technique to smooth images while preserving edges, where separable Gaussian coefficients at a point are weighted jointly by the spatial distance and the intensity distance between its neighbours. For a real valued discrete image $f : \Omega \to \mathbb{R}$, bilateral filtering is formalized as

$$\mathrm{BL}(f)(\mathbf{x}; \sigma_s, \sigma_r) = \frac{\sum_{\mathbf{y} \in N(\mathbf{x})} f(\mathbf{y}) e^{-\frac{\|\mathbf{x}-\mathbf{y}\|^2}{2\sigma_s^2}} e^{-\frac{|\bar{f}(\mathbf{x})-\bar{f}(\mathbf{y})|}{2\sigma_r^2}}}{\sum_{\mathbf{y} \in N(\mathbf{x})} e^{-\frac{\|\mathbf{x}-\mathbf{y}\|^2}{2\sigma_s^2}} e^{-\frac{|\bar{f}(\mathbf{x})-\bar{f}(\mathbf{y})|^2}{2\sigma_r^2}}}$$

(a) $p = 1$ (Log-Euclidean median)

(b) $p = 2$ (Log-Euclidean mean)

(c) $p = \infty$ (Log-Euclidean minimax center)

FIGURE 2. Quaternion image filtering using Log-Euclidean L^p averaging of RGB+Depth image, with three values of p. Average is computed in a window of 11×11 pixels.

and it requires only two easily tunable parameters: a scale parameter related to the size σ_s and a scale parameter related to the contrast σ_r of the image features to be preserved. The neigbourhood of filter N is typically a square window of $[2\sigma_s - 1 \times 2\sigma_s - 1]$ pixels. A systematic study on the theory and applications of bilateral filtering can be found in [38]. As it was shown in [21], bilateral filtering is strongly related to other image filtering techniques such as weighted least squares filtering, robust estimation filtering and anisotropic

(a) $p = 1$ (Riemannian median)

(b) $p = 2$ (Riemannian mean)

(c) $p = \infty$ (Riemannian minimax center)

FIGURE 3. Quaternion image filtering using Riemannian L^p averaging of RGB+Depth image, with three values of p. Average is computed in a window of 11×11 pixels.

diffusion. In particular, bilateral filtering is a discrete filter equivalent asymptotically to Perona and Malik PDE equation [40].

The extension of bilateral filtering to 2D quaternion images $f_{\mathbf{q}}$ is rather natural using our methods of geometric averaging of a set of quaternions $\mathbb{E}(\mathfrak{Q}, \mathbf{A})$. The corresponding algorithm is formulated as follows:

$$\mathrm{BL}(f_{\mathbf{q}})(\mathbf{x}; \sigma_s, \sigma_r) = \{\mathbb{E}(\{f_{\mathbf{q}}(\mathbf{y})\},\ \{\alpha_{\mathbf{x}}(\mathbf{y}; \sigma_s, \sigma_r)\});\ \mathbf{y} \in N(\mathbf{x})\}, \qquad (4.2)$$

(a) $f_{\mathbf{q}} = (\mathbf{1}, f_R, f_G, f_B)$

(b-1) $\mathrm{BL}(f_{\mathbf{q}})(\sigma_s, \sigma_i)$ $\sigma_r = 0.9$, $p = 2$

(c-1) $\mathrm{BL}(f_{\mathbf{q}})(\sigma_s, \sigma_r)$ $\sigma_r = 0.1$, $p = 2$

(b-2) $\mathrm{BL}(f_{\mathbf{q}})(\sigma_s, \sigma_i)$ $\sigma_r = 0.9$, $p = 2$

(c-2) $\mathrm{BL}(f_{\mathbf{q}})(\sigma_s, \sigma_r)$ $\sigma_r = 0.1$, $p = 2$

(b-3) $\mathrm{BL}(f_{\mathbf{q}})(\sigma_s, \sigma_r)$ $\sigma_r = 0.9$, $p = 1$

(c-3) $\mathrm{BL}(f_{\mathbf{q}})(\sigma_s, \sigma_i)$ $\sigma_r = 0.1$, $p = 1$

(b-4) $\mathrm{BL}(f_{\mathbf{q}})(\sigma_s, \sigma_i)$ $\sigma_r = 0.9$, $p = 1$

(c-4) $\mathrm{BL}(f_{\mathbf{q}})(\sigma_s, \sigma_r)$ $\sigma_r = 0.1$, $p = 1$

FIGURE 4. Quaternion bilateral filtering $\mathrm{BL}(f_{\mathbf{q}})$ of noisy color image (with $\sigma_s = 5$): (a) original image (256×256 pixels); (b-) quaternion range penalization $\sigma_r = 0.9$, (c-) quaternion range penalization $\sigma_r = 0.1$; (-1) Log-Euclidean quaternion mean, (-2) Fréchet-Karcher quaternion barycenter, (-3) Log-Euclidean quaternion median, (-4) Fermat-Weber quaternion point.

such that

$$\mathbb{E}\left(\{f_{\mathbf{q}}(\mathbf{y})\},\ \{\alpha_{\mathbf{x}}(\mathbf{y};\sigma_s,\sigma_r)\}\right) = \arg\min_{\mathbf{q}\in\mathbb{H}} \sum_{\mathbf{y}\in N(\mathbf{x})} \alpha_{\mathbf{x}}(\mathbf{y};\sigma_s,\sigma_r)\, \mathrm{dist}^2_{\mathbb{H}^*}(\mathbf{q}, f_{\mathbf{q}}(\mathbf{y})), \tag{4.3}$$

FIGURE 5. Quaternion bilateral filtering $\mathrm{BL}(f_{\mathbf{q}})$ of RGB+NIR and RGB+Depth images of Fig. 1. In both cases it consists in Log-Euclidean mean averaging, with $\sigma_s = 5$ and $\sigma_r = 0.1$.

FIGURE 6. Marginal bilateral filtering of RGB and Depth images of Fig. 1. The four components have been filtered with $\sigma_s = 5$ and $\sigma_r = 0.1$.

where $\alpha_{\mathbf{x}}(\mathbf{y}; \sigma_s, \sigma_r)$ is the set of spatially local adaptive bilateral weights for pixel $\mathbf{x}$ computed as

$$\alpha_{\mathbf{x}}(\mathbf{y}; \sigma_s, \sigma_i) = \frac{1}{\widetilde{W}_{\mathbf{x}}} e^{-\frac{(x_1-y_1)^2+(x_2-y_2)^2}{2\sigma_s^2}} e^{-\frac{\mathrm{dist}^2_{\mathbb{H}^*}(\bar{f}_{\mathbf{q}}(\mathbf{y}), \bar{f}_{\mathbf{q}}(\mathbf{x}))}{2\sigma_r^2}}, \tag{4.4}$$

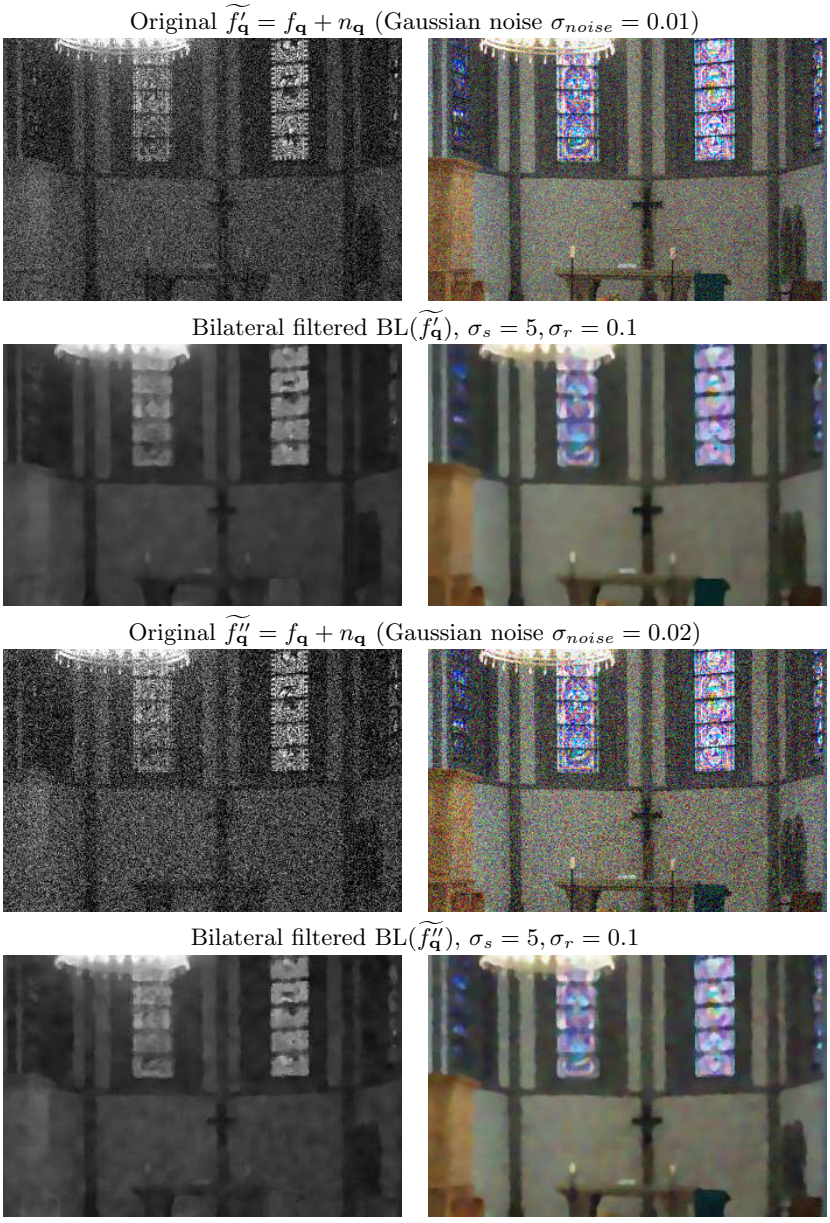

FIGURE 7. Quaternion bilateral filtering $\mathrm{BL}(f_{\mathbf{q}})$ of Gaussian-noise corrupted RGB+NIR image, using Log-Euclidean mean averaging, with $\sigma_s = 5$ and $\sigma_r = 0.1$.

and where $\widetilde{W}_{\mathbf{x}}$ is the normalization factor; i.e., $\widetilde{W}_{\mathbf{x}} = \sum_{\mathbf{y} \in N(\mathbf{x})} \alpha_{\mathbf{x}}(\mathbf{y}; \sigma_s, \sigma_r)$. The pair of width parameters (σ_s, σ_r) in (4.4) defines the filtering scales, where σ_s is the spatial (or size) scale and σ_i the "quaternion range" scale.

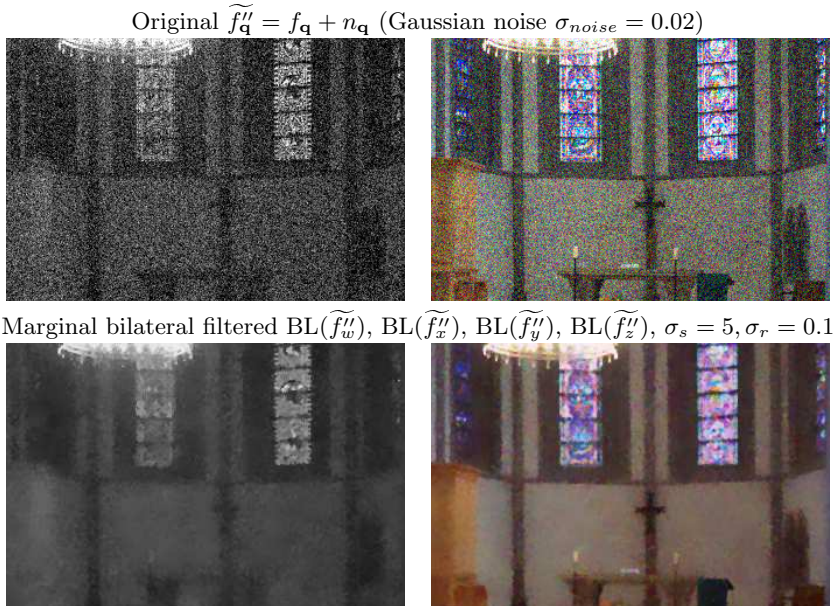

FIGURE 8. Marginal bilateral filtering $\mathrm{BL}(f_{\mathbf{q}})$ of Gaussian-noise corrupted RGB and NIR images. The four components have been filtered with $\sigma_s = 5$ and $\sigma_r = 0.1$.

The quaternion range distances in the expression (4.4) are obviously computed as the Riemannian distance on $\mathbb{H}^*$. However, in order to achieve a robust estimation, this penalization distance is computed in a pre-filtered version of the quaternion image, which is denoted by $\bar{f}_{\mathbf{q}}$, i.e.,

$$\mathrm{dist}_{\mathbb{H}^*}\left(\bar{f}_{\mathbf{q}}(\mathbf{y}), \bar{f}_{\mathbf{q}}(\mathbf{x})\right) = \left\|\log\left(\bar{f}_{\mathbf{q}}(\mathbf{y})^{-\frac{1}{2}}\bar{f}_{\mathbf{q}}(\mathbf{x})\bar{f}_{\mathbf{q}}(\mathbf{y})^{-\frac{1}{2}}\right)\right\|,$$

where $\bar{f}_{\mathbf{q}}$ is typically obtained by a fast marginal mean filter for each component of the quaternion image using a window of size 3×3 pixels. The computation of the weights from $\bar{f}_{\mathbf{q}}$, a regularized version of the image, leads to robustness against noise. This approach is well known in nonlinear diffusion [20]. Instead of the marginal mean, any other fast pre-filter can be applied, e.g., marginal median. Note that the Riemannian mean in (4.3) is computed from the original values of $f_{\mathbf{q}}$ (minimizing the square of the geodesic distance) and only the adaptive weights are estimated from $\bar{f}_{\mathbf{q}}$. Note also that in the iterative algorithms for the Riemannian mean, the weights at each point are the same for all the iterations.

The Riemannian mean estimator $\mathbb{E}(\cdot)$ can be replaced by any other Riemannian L^p center of mass. The general procedure is summarized in Algorithm 1. We can also consider the Log-Euclidean L^p center of mass for bilateral filtering. In this latter case, the Riemannian distance should be replaced by the Log-Euclidean distance, see Algorithm 2. In computational

terms, it is obvious that the Log-Euclidean bilateral filtering is more efficient since only involves vector algorithms on the pixelwise quaternion logarithm image. In particular, the case L^2 involves a straightforward computation of the mean without the need of an iterative algorithm.

input : Quaternion image $f_{\mathbf{q}}(\mathbf{x})$, type of center-of-mass p, filtering parameters σ_s, σ_r
output: Filtered quaternion image $\mathrm{BL}(f_{\mathbf{q}})(\mathbf{x})$

begin
- Compute cardinal of neighborhood: $N \leftarrow (2\sigma_s - 1)(2\sigma_s - 1)$;
- Compute marginal median filtered image: $\bar{f}_{\mathbf{q}}(x)$;
- Compute spatial penalization weights for $\mathbf{y} \in Nb(\mathbf{0})$ (same for all pixels): $\alpha(\mathbf{y}) \leftarrow \exp\left(-\|\mathbf{y}\|/2\sigma_s^2\right)$;
- **for** $\mathbf{x} \in \Omega$ **do**
  - $i \leftarrow 1$;
  - **for** $\mathbf{y} \in Nb(\mathbf{x})$ **do**
    - Compute range penalization weights using quaternion distances from $\bar{f}_{\mathbf{q}}(x)$: $\alpha_{\mathbf{x}}(\mathbf{y}) \leftarrow \exp\left(-\mathrm{dist}^2_{\mathbb{H}^*}(\bar{f}_{\mathbf{q}}(\mathbf{y}), \bar{f}_{\mathbf{q}}(\mathbf{x}))/2\sigma_r^2\right)$;
    - Get original quaternion image value: $\mathbf{q}_i = f_{\mathbf{q}}(x)$;
    - $i \leftarrow i + 1$;
  - **end**
  - **for** $i \leftarrow 1$ **to** N **do**
    - Compute normalized weights: $\alpha_i \leftarrow (\alpha(\mathbf{y})\alpha_{\mathbf{x}}(\mathbf{y}))/\sum_{\mathbf{y}\in Nb(\mathbf{x})} \alpha_{\mathbf{x}}(\mathbf{y})$;
  - **end**
  - Compute Riemannian L^p center-of-mass $\overline{\mathbf{q}}$ for set of quaternions $\{\mathbf{q}_i\}_{i=1}^N$ using weights $\{\alpha_i\}_{i=1}^N$: **switch** p **do**
    - **case** 1 Iterative algorithm from (3.10) **case** 2 Iterative algorithm from (3.9)**case** $2 < p < \infty$ Iterative algorithm from (3.11)
  - **end**
  - Quaternion center-of-mass to image result: $\mathrm{BL}(f_{\mathbf{q}})(\mathbf{x}) \leftarrow \overline{\mathbf{q}}$
- **end**

end

Algorithm 1: Quaternion Riemannian L^p bilateral filtering.

In order to illustrate the behavior of quaternion bilateral filtering, let us consider firstly an example of noisy color image (f_R, f_G, f_B). Fig. 4 depicts a systematic comparison of the effect of quaternion bilateral filtering, for a given spatial size of bilateral filter $\sigma_s = 5$. More precisely, the example compares, on the one hand, the results obtained using Log-Euclidean quaternion averaging for $p = 2$ and $p = 1$ with respect to those obtained using Fréchet-Karcher barycenter and Fermat-Weber point; on the other, the effect of the quaternion range penalization $\sigma_r = 0.9$ and $\sigma_r = 0.1$. As expected, for all the examples, high values of σ_i produce similar blurring results to the spatially-invariant Gaussian filter; on the contrary, a typical value of $\sigma_r = 0.1$ is a good trade-off to achieve the adaptive effect of bilateral kernels, which preserves

input : Quaternion image $f_{\mathbf{q}}(\mathbf{x})$, type of Log-Euclidean center-of-mass p, filtering parameters σ_s, σ_r
output: Filtered quaternion image $\mathrm{BL}(f_{\mathbf{q}})(\mathbf{x})$

begin
- Compute cardinal of neighborhood: $N \leftarrow (2\sigma_s - 1)(2\sigma_s - 1)$;
- Compute pixelwise logarithm of quaternion image: $f_{\mathbf{q}}^{\log}(\mathbf{x}) \leftarrow \log(f_{\mathbf{q}}(\mathbf{x}))$;
- Compute marginal median filtered image from $f_{\mathbf{q}}^{\log}(\mathbf{x})$: $\bar{f}_{\mathbf{q}}^{\log}(x)$;
- Compute spatial penalization weights for $\mathbf{y} \in Nb(\mathbf{0})$ (same for all pixels): $\alpha(\mathbf{y}) \leftarrow \exp\left(-\|\mathbf{y}\|/2\sigma_s^2\right)$;
- **for** $\mathbf{x} \in \Omega$ **do**
  - $i \leftarrow 1$;
  - **for** $\mathbf{y} \in Nb(\mathbf{x})$ **do**
    - Compute range penalization weights using vector distances from $\bar{f}_{\mathbf{q}}^{\log}(x)$: $\alpha_{\mathbf{x}}(\mathbf{y}) \leftarrow \exp\left(-\|\bar{f}_{\mathbf{q}}^{\log}(\mathbf{y}) - \bar{f}_{\mathbf{q}_{\mathbf{q}}}^{\log}(\mathbf{x})\|^2/2\sigma_r^2\right)$;
    - Get original logarithmic image value: $\eta_i = f_{\mathbf{q}}^{\log}(\mathbf{x})$;
    - $i \leftarrow i + 1$;
  - **end**
  - **for** $i \leftarrow 1$ **to** N **do**
    - Compute normalized weights: $\alpha_i \leftarrow (\alpha(\mathbf{y})\alpha_{\mathbf{x}}(\mathbf{y}))/\sum_{\mathbf{y}\in Nb(\mathbf{x})} \alpha_{\mathbf{x}}(\mathbf{y})$;
  - **end**
  - Compute L^p center-of-mass $\overline{\eta}$ for set of 4D vectors $\{\eta_i\}_{i=1}^N$ using weights $\{\alpha_i\}_{i=1}^N$: **switch** p **do**
    - **case** 1 $\overline{\eta} = \sum_{i=1}^N \alpha_i \eta_i$ **case** 2 Iterative algorithm from (3.6)
  - **end**
  - Center-of-mass to image result: $f_\eta(\mathbf{x}) \leftarrow \overline{\eta}$
- **end**
- Compute pixelwise exponential of image: $\mathrm{BL}(f_{\mathbf{q}})(\mathbf{x}) \leftarrow \exp(f_\eta(\mathbf{x}))$;

end

Algorithm 2: Quaternion Log-Euclidean L^1/L^2 bilateral filtering

appropriately the image edges. Concerning the averaging algorithm, we observe that the results are rather similar; the Riemannian mean and median yielding both more colorful values. An important conclusion from the example is the fact that the choice of $p = 1$ or $p = 2$ has a relatively low impact on the bilateral filtering since, by definition, bilateral filtering is robust against outliers (corresponding weights depending on the quaternion range are very slow). Consequently the estimation using L^2 takes into account this effect to lead to a robust averaging.

We can naturally apply quaternion bilateral filtering to regularize color + temperature and color + distance images. Fig. 5 gives the results obtained for the images of Fig. 1. We observe how color and temperature/distance structures are simultaneously simplified into similar geometric regions where the contours are well preserved. In order to illustrate the interest of the

present approach, we have included in Fig. 6 the result of marginal bilateral filtering of RGB and depth images, i.e., the four components have been filtered independently using the same scale parameters as in Fig. 5. As we can observe from the depth component, the quaternion bilateral filtering involves a filtering effect which is driven by the regular parts of the RGB components. In the case of the marginal approach, without interaction between the components, the filtering of the depth is very unsatisfactory.

Finally, let us consider a last example given in Fig. 7, to illustrate the denoising performance of quaternion bilateral filtering. Two noisy versions of the color+temperature image are considered (i.e., the initial quaternionic image $f_{\mathbf{q}}$ has been corrupted with Gaussian noise of standard deviation $\sigma_{noise} = 0.01$ for $\widetilde{f'_{\mathbf{q}}}$ and $\sigma_{noise} = 0.02$ for $\widetilde{f''_{\mathbf{q}}}$). Images are bilateral filtered using the same scale parameters with Log-Euclidean mean estimator. The restored results can be compared to the one obtained for the unnoisy image in Fig. 5, which proves the excellent robustness of bilateral filtering for image denoising. For the case of image $\widetilde{f''_{\mathbf{q}}}$, we have also included in Fig. 8 the result obtained by a marginal bilateral processing of the four components. As we can observe, the quaternion bilateral processing clearly outperforms the marginal processing. More precisely, the marginally denoised components present severe drawbacks: the NIR component is poorly restored and the RGB components have introduced notably false colors.

5. Conclusions and Perspectives

We have introduced two families of algorithms for the computation of the weighted mean of quaternions on the intrinsic geometry of $\mathbb{H}^*$. The Log-Euclidean framework is simply Euclidean processing in the logarithmic domain (i.e., Lie algebra of $\mathbb{H}^*$) and consequently is computationally simpler than the Riemannian L^p center of mass on $\mathbb{H}^*$, which is based on gradient flow algorithms. We notice also that quaternion exponential and logarithm are relatively inexpensive to compute, particularly compared with the cost of those operations for other charts on matrices Lie groups which requires matrix exponential and matrix logarithm. This point supports the fact that geometric averaging in $SO(3)$ or $SU(2)$ can be done more efficiently working with unit quaternions (a subgroup of $\mathbb{H}^*$), which can be implemented using the algorithms here discussed.

The averaging statistics can be used for four-components image filtering and in particular, we have considered the case of the extension of bilateral filtering to quaternionic images. From the empirical examples, we can conclude that both families of algorithms produce relatively similar results in processing color + temperature / distance images.

Aiming at developing a more theoretically sound approach for adaptive color + distance image filtering, we will consider the geometric flow PDE associated to the extension of Laplace-Beltrami framework [44, 31] for

quaternion-valued images. It mainly involves an embedding of the 2D quaternion image into a product manifold, i.e.,

$$f_{\mathbf{q}}(x_1, x_2) \mapsto (X^1 = x_1, X^2 = x_2, X^3 = f_{\mathbf{q}}(x, y)) \in \mathbb{R}^2 \times \mathbb{H},$$

then, using the underlying product metric of arc length element equal to $ds^2 = ds^2_{space} + \alpha ds^2_{\mathbb{H}^*} = dx_1^2 + dx_2^2 + \alpha df^2_{\mathbf{q}}$, $\alpha > 0$, the numerical solution of the corresponding Laplace-Beltrami flow can be obtained by finite difference numerical schemas.

From a more applicative perspective, our goal is to work on the problem of nonzero quaternion interpolation, in both Log-Euclidean and Riemannian frameworks, for simultaneous color + distance image interpolation (image resizing, image inpainting, etc.)

References

[1] R. Abłamowicz, G. Sobczyk, (Editors) *Lectures on Clifford (Geometric) Algebras and Applications*. Birkhäuser, Boston (2004).

[2] B. Afsari, *Riemannian L^p center of mass: existence, uniqueness and convexity*. Proc. of the American Mathematical Society **139** (2) (2010), 655–673.

[3] B. Afsari, R. Tron, R. Vidal, *On The Convergence of Gradient Descent for Finding the Riemannian Center of Mass*. arXiv:1201.0925 (2011).

[4] S. L. Altmann, *Rotations, quaternions, and double groups*. The Clarendon Press, Oxford University Press, New York (1986)

[5] M. Arnaudon, C. Dombry, A. Phan, L. Yang, *Stochastic algorithms for computing means of probability measures*. arXiv:1106.5106 (2011).

[6] M. Arnaudon, F. Nielsen, *On approximating the Riemannian 1-center*. Computational Geometry 46 (1) (2013), 93–104.

[7] V. Arsigny, X. Pennec, N. Ayache, *Bi-Invariant Means in Lie Groups. Application to Left-Invariant Polyaffine Transformations*. INRIA Research Report No 5885 (2006).

[8] V. Arsigny, P. Fillard, X. Pennec, N. Ayache, *Geometric Means in a Novel Vector Space Structure on Symmetric Positive-Definite Matrices*. SIAM. J. Matrix Anal. & Appl. **29** (2007), 328–347.

[9] M. Bădoiu, K. L. Clarkson, *Smaller core-sets for balls*. In: Proc. of the fourteenth annual ACM-SIAM symposium on Discrete algorithms (SIAM) (2003), pp. 801–802.

[10] F. Barbaresco, *Geometric Radar Processing based on Fréchet Distance: Information Geometry versus Optimal Transport Theory*. In: Proc. of International Radar Conference (IRS'11) (2011).

[11] F. Barbaresco, *Information Geometry of Covariance Matrix: Cartan-Siegel Homogenous Bounded Domains, Mostow/Berger Fibration and Fréchet Median*. In: (Nielsen, F., Bhatia, R., Eds.) Matrix Information Geometries, Springer (2013).

[12] M. L. Barberis, *Hypercomplex Structures on Four-dimensional Lie Groups*. Proc. of the American Mathematical Society **125** (4) (1998), 1043–1054.

[13] R. Bhatia, J. Holbrook, *Riemannian geometry and matrix geometric means*. Linear Algebra and its Applications **413** (2006), 594–618.

[14] R. Bhattacharya, V. Patrangenaru, *Large sample theory of intrinsic and extrinsic sample means on manifolds, I.* Ann. Statist. **31** (1) (2003), 1–29.

[15] S. Bonnabel, R. Sepulchre, *Geometric distance and mean for positive semi-definite matrices of fixed rank.* SIAM. J. Matrix Anal. & Appl. **31** (2009), 1055–1070.

[16] S. Bonnabel, *Stochastic gradient descent on Riemannian manifolds.* arXiv:1111.5280 (2012).

[17] M. Brown, S. Süsstrunk, *Multispectral SIFT for Scene Category Recognition.* In: Proc. of International Conference on Computer Vision and Pattern Recognition (CVPR'11) (2011).

[18] S. Buchholz, G. Sommer *On Averaging in Clifford Groups.* In: Proc. of the 6th Int. Conf. on Computer Algebra and Geometric Algebra with Applications (IWMM'04/GIAE'04) LNCS 3519, (2005), 183–198.

[19] S. R. Buss, J. Fillmore, *Spherical Averages and Applications to Spherical Splines and Interpolation.* ACM Transactions on Graphics **20** (2001), 95–126.

[20] F. Catte, P. -L. Lions, J. -M. Morel, T. Coll, *Image selective smoothing and edge detection by nonlinear diffusion.* SIAM Journal on Numerical Analysis **29** (1992), 182–193.

[21] M. Elad *On the Origin of the Bilateral Filter and Ways to Improve It.* IEEE Trans. on Image Processing **11** (2002), 1141–1151.

[22] S. Fiori, *On vector averaging over the unit hyphersphere.* Digital Signal Process **19** (4) (2009), 715–725.

[23] S. Fiori, T. Toshihisa, *An Algorithm to Compute Averages on Matrix Lie Groups.* IEEE Trans. on Signal Processing **57** (12) (2009), 4734–4743.

[24] P. T. Fletcher, S. Venkatasubramanian, S. Joshi, *The geometric median on riemannian manifolds with application to robust atlas estimation.* NeuroImage **45** (1) (2009), S143– S152.

[25] M. Fréchet, *Les élements aléatoires de nature quelconque dans un espace distancié.* Ann. Inst. H. Poincaré **10** (1948), 215–310.

[26] C. Gramkow, *On Averaging Rotations.* International Journal of Computer Vision **42** (1/2) 2001, 7–16.

[27] R. Hartley, J. Trumpf, Y. Dai, *Rotation averaging and weak convexity.* In: Proc. of the 19th International Symposium on Mathematical Theory of Networks and Systems (MTNS'10) (2010), pp. 2435–2442.

[28] H. Helmholtz von, *Handbuch der PsychologishenOptik.* Voss, Hamburg, (1896).

[29] H. Karcher, *Riemann center of mass and mollifier smoothing.* Communications on Pure and Applied Mathematics **30** (1997), 509–541.

[30] D. G. Kendall, *Shape manifolds, Procrustean metrics, and complex projective spaces.* Bulletin of the London Mathematical Society **16** (1984), 18–121.

[31] R. Kimmel, *Images as Embedded Maps and Minimal Surfaces: Movies, Color, Texture, and Volumetric Medical Images.* International Journal of Computer Vision **39** (2) (2000), 111–129.

[32] K. Krakowski, K. Hüper, J. Manton, *On the computation of the karcher mean on spheres and special orthogonal groups.* In: RoboMat 2007, Workshop on Robotics and Mathematics (2007)

[33] H. W. Kuhn, R. E. Kuenne, *An efficient algorithm for the numerical solution of the generalized Weber problem in spatial economics*. J. Regional Sci. **4** (1962), 21–34.

[34] H. Le, *Estimation of Reimannian barycenters*. LMS Journal of Computation and Mathematics **7** (2004), 193–200.

[35] M. Moakher, *Means and averaging in the group of rotations*. SIAM J. Matrix Anal. Appl. **24** (1) (2002), 1–16.

[36] M. Moakher, *A differential geometry approach to the geometric mean of symmetric positive definite matrices*. SIAM J. Matrix Anal. & Appl. **26** (2005), 735–747.

[37] L. M. Ostresh, *On the convergence of a class of iterative methods for solving the Weber location problem*. Operations Research **26** (1978), 597–609.

[38] S. Paris, Kornprobst, P. J. Tumblin, F. Durand, *Bilateral Filtering: Theory and Applications*. Foundations and Trends in Computer Graphics and Vision **4** (2008), 1–73.

[39] X. Pennec, *Computing the mean of geometric features: application to the mean rotation*. INRIA Research Report No 3371 (1998).

[40] P. Perona, J. Malik, *Scale-Space and Edge Detection Using Anisotropic Diffusion*. IEEE Trans. Pattern Anal. Mach. Intell. **12** (1990), 629–639.

[41] A. Sarlette, R. Sepulchre, *Consensus optimization on manifolds*. SIAM J. Control Optim. **48** (1) (2009), 56—76.

[42] E. Schrödinger, *Grundlinien einer theorie der farbenmetrik in tagessehen*. Ann. Physik **63** (1920), 481.

[43] K. Shoemake, *Animating rotation with quaternion curves*. In: Proc of 12th Conference on Computer Graphics and Interactive Techniques (SIGGRAPH'85) ACM Press (1985).

[44] N. Sochen, Y. Y. Zeevi, *The Beltrami geometrical framework of color image processing*. In: Proc. of IEEE International Conference Acoustics, Speech, and Signal Processing (ICASSP'99), Vol. 6, 3301–3304 (1999).

[45] J. Sturm, S. Magnenat, N. Engelhard, F. Pomerleau, F. Colas, W. Burgard, D. Cremers, R. Siegwart, *Towards a benchmark for RGB-D SLAM evaluation*. In: Proc. of the RGB-D Workshop on Advanced Reasoning with Depth Cameras at Robotics: Science and Systems Conf. (2011).

[46] C. Tomasi, R. Manduchi, *Bilateral filtering for gray and color images*. In: Proc. of 6th Int. Conf. Computer Vision (ICCV'98) (1998), pp. 839–846.

[47] E. Weiszfeld, *Sur le point pour lequel la somme des distances de n points données est minimum*. Tohoku Math. J. **43** (1937), 355–386.

[48] L. Yang, *Riemannian median and its estimation*. LMS Journal of Computations and Mathematics **13** (2010), 461–479.

[49] L. Yang, *Medians of probability measures in Riemannian manifolds and applications to radar target detection*. Ph. D. Thesis, Université de Poitiers (2011). "http://tel.archives-ouvertes.fr/tel-00664188/"

Jesús Angulo
CMM-Centre de Morphologie Mathématique,
Mathématiques et Systèmes,
MINES ParisTech
35, rue Saint-Honoré; 77300 Fontainebleau; France
e-mail: jesus.angulo@mines-paristech.fr

Received: December 19, 2013.
Accepted: September 27, 2013.